Sub-wavelength grating components for integrated optics applications on SOI chips

Valentina Donzella,[1*] Ahmed Sherwali,[1] Jonas Flueckiger,[1] Sahba Talebi Fard,[1] Samantha M. Grist,[1] and Lukas Chrostowski[1]

[1]*Department of Electrical and Computer Engineering, University of British Columbia, Canada*
**valedonz@ece.ubc.ca*

Abstract: In this paper we demonstrate silicon on insulator (SOI) sub-wavelength grating (SWG) optical components for integrated optics and sensing. Light propagation in SWG devices is studied and realized with no cladding on top of the waveguide. In particular, we focused on SWG bends, tapers and directional couplers, all realized with compatible geometries in order to be used as building blocks for more complex integrated optics devices (interferometers, switches, resonators, etc.). Fabricated SWG tapers for TE and TM polarizations are described; they allow for connecting SWG devices to regular strip waveguides with loss lower than 1 dB per taper. Our SWG directional coupler presents a very compact design and a negligible wavelength dependence of its crossover length (and as a consequence of its coupling coefficient, κ), over a 40 nm bandwidth. This wavelength flatten response represents a bandwidth enhancement with respect to standard directional couplers (made using strip or rib waveguides), in particular for the TE mode. SWG bends are demonstrated, their loss dependence on radius is analyzed, and fabricated bends have a loss in the range 0.8-1.6 dB per 90 degrees bend. Simulated and measured results show promise for large-scale fabrication of complex optical devices and high sensitivity sensors based on SWG waveguides with engineered optical properties, tailored to specific applications.

OCIS codes: (230.0230) Optical devices; (230.3120) Integrated optics devices; (230.3990) Micro-optical devices; (230.7370) Waveguides; (350.2770) Gratings.

References and links

1. M. Hochberg, N. C. Harris, D. Ran, Z. Yi, A. Novack, X. Zhe, and T. Baehr-Jones, "Silicon photonics: the next fabless semiconductor industry," IEEE Solid-State Circ. Mag. **5**(1), 48–58 (2013).
2. R. Soref, "The past, present, and future of silicon photonics," IEEE J. Sel. Top. Quantum Electron. **12**(6), 1678–1687 (2006).
3. L. Chrostowski and M. Hochberg, *Silicon Photonics Design* (Cambridge University Press, 2014)
4. S. Selvaraja, G. Murdoch, A. Milenin, C. Delvaux, P. Ong, S. Pathak, D. Vermeulen, G. Sterckx, G.Winroth, P. Verheyen, G. Lepage, W. Bogaerts, R. Baets, J. Van Campenhout and P. Absil, "Advanced 300-mm waferscale patterning for silicon photonics devices with record low loss and phase errors," 17th Opto-Electronics and Communications Conference-OECC, PDP2–2, (2012).
5. Y. Liu, R. Ding, M. Gould, T. Baehr-Jones, Y. Yang, Y. Ma, Y. Zhang, A. Lim, T. Y. Liow, S. Teo, G. Q. Lo, and M. Hochberg, "30GHz silicon platform for photonics system," IEEE Optical Interconnects Conference (2013).
6. B. Jalali and S. Fathpour, "Silicon photonics," IEEE J. Lightw. Tech. **24**(12), 4600–4615 (2006).
7. R. Soref, "Silicon photonics: a review of recent literature," Silicon. **2**(1), 1–6 (2010).
8. S. Talebifard, S. M. Grist, V. Donzella, S. A. Schmidt, J. Flueckiger, X. Wang, W. Shi, A. Millspaugh, M. Webb, D. M. Ratner, K. C. Cheung, and L. Chrostowski, "Label-free silicon photonic biosensors for use in clinical diagnostics," SPIE OPTO 862909 (2014).
9. S. M. Grist, S. A. Schmidt, J. Flueckiger, V. Donzella, W. Shi, S. Talebi Fard, J. T. Kirk, D. M. Ratner, K. C. Cheung, and L. Chrostowski, "Silicon photonic micro-disk resonators for label-free biosensing," Opt. Express **21**(7), 7994–8006 (2013).

#214987 - $15.00 USD Received 1 Jul 2014; revised 7 Aug 2014; accepted 14 Aug 2014; published 22 Aug 2014

10. V. Donzella, S. Talebi Fard, and L. Chrostowski, "Modelling of asymmetric slot racetracks for improved bio-sensors performance," Numerical Simulation of Optoelectronic Devices (NUSOD), 2013 13th International Conference on pp.25, 26 (2013).
11. X. Wang, J. Flueckiger, S. Schmidt, S. Grist, S. T. Fard, J. Kirk, M. Doerfler, K. C. Cheung, D. M. Ratner, and L. Chrostowski, "A silicon photonic biosensor using phase-shifted Bragg gratings in slot waveguide," J Biophotonics **6**(10), 821–828 (2013).
12. S. Talebifard, V. Donzella, S. A. Schmidt, D. M. Ratner, R. J. Bojko, and L. Chrostowski, "Sensitivity analysis of thin waveguide SOI ring resonators for sensing applications," IEEE Photonics Conference (IPC) pp.616–617, (2013).
13. J. H. E. Kim, L. Chrostowski, E. Bisaillon, and D. V. Plant, "DBR, Sub-wavelength grating, and photonic crystal slab Fabry-Perot cavity design using phase analysis by FDTD," Opt. Express **15**(16), 10330–10339 (2007).
14. D. Nir, Z. Weissman, S. Ruschin, and A. Hardy, "Periodically segmented waveguides in Ti:$LiNbO_3$," Opt. Lett. **19**(12), 880–882 (1994).
15. K. Thyagarajan, C. W. Chien, R. V. Ramaswamy, H. S. Kim, and H. C. Cheng, "Proton-exchange periodically segmented waveguides in $LiNbO_3$," Opt. Lett. **19**(12), 880 (1994).
16. P. J. Bock, P. Cheben, J. H. Schmid, J. Lapointe, A. Delâge, D. X. Xu, S. Janz, A. Densmore, T. J. Hall, and T. J. Hall, "Subwavelength grating crossings for silicon wire waveguides," Opt. Express **18**(15), 16146–16155 (2010).
17. X. Wang, S. Grist, J. Flueckiger, N. A. Jaeger, and L. Chrostowski, "Silicon photonic slot waveguide Bragg gratings and resonators," Opt. Express **21**(16), 19029–19039 (2013).
18. R. Halir, A. Maese-Novo, A. Ortega-Moñux, I. Molina-Fernández, J. G. Wangüemert-Pérez, P. Cheben, D.-X. Xu, J. H. Schmid, and S. Janz, "Colorless directional coupler with dispersion engineered sub-wavelength structure," Opt. Express **20**(12), 13470–13477 (2012).
19. P. Cheben, P. J. Bock, J. H. Schmid, J. Lapointe, S. Janz, D. X. Xu, A. Densmore, A. Delâge, B. Lamontagne, and T. J. Hall, "Refractive index engineering with subwavelength gratings for efficient microphotonic couplers and planar waveguide multiplexers," Opt. Lett. **35**(15), 2526–2528 (2010).
20. X. Wang, Y. Wang, J. Flueckiger, R Bojko, A. Liu, A. Reid, J. Pond, N.A. F. Jaeger, and L. Chrostowski, "Precise control of the coupling coefficient through destructive interference in silicon waveguide Bragg gratings," submitted.
21. D. Ortega, J. M. Aldariz, J. M. Arnold, and J. S. Aitchison, "Analysis of "quasi-modes" in periodic segmented waveguides," J. Lightw. Tech. **17**(2), 369–375 (1999).
22. S. T. Fard, V. Donzella, S. A. Schmidt, J. Flueckiger, S. M. Grist, P. Talebi Fard, Y. Wu, R. J. Bojko, E. Kwok, N. A. Jaeger, D. M. Ratner, and L. Chrostowski, "Performance of ultra-thin SOI-based resonators for sensing applications," Opt. Express **22**(12), 14166–14179 (2014).
23. *www.lumerical.com*
24. K. O. Hill and G. Meltz, "Fiber Bragg grating technology fundamentals and overview," IEEE J Lightw. Tech. **15**(8), 1263–1276 (1997).
25. Y. Chen, J. Feng, Z. Zhou, C. J. Summers, D. S. Citrin, and J. Yu, "Simple technique to fabricate microscale and nanoscale silicon waveguide devices," Front. Optoelectron. China **2**(3), 308–311 (2009).
26. R. J. Bojko, J. Li, L. He, T. Baehr-Jones, M. Hochberg, and Y. Aida, "Electron beam lithography writing strategies for low loss, high confinement silicon optical waveguides," J. Vac. Sci. Technol. B **29**(6), 06F309 (2011).
27. Y. Wang, J. Flueckiger, C. Lin, and L. Chrostowski, "Fully-etched grating coupler with low back reflection," SPIE Photonics North 89150U (2013).
28. D. M. Beggs, T. P. White, L. O'Faolain, and T. F. Krauss, "Ultracompact and low-power optical switch based on silicon photonic crystals," Opt. Lett. **33**(2), 147–149 (2008).
29. D.-X. Xu, M. Vachon, A. Densmore, R. Ma, A. Delâge, S. Janz, J. Lapointe, Y. Li, G. Lopinski, D. Zhang, Q. Y. Liu, P. Cheben, and J. H. Schmid, "Label-free biosensor array based on silicon-on-insulator ring resonators addressed using a WDM approach," Opt. Lett. **35**(16), 2771–2773 (2010).
30. T. Lee, D. Lee, and Y. Chung, "Design and simulation of fabrication-error-tolerant triplexer based on cascaded Mach–Zehnder inteferometers," IEEE Photon. Technol. Lett. **20**(1), 33–35 (2008).
31. M. Thorhauge, L. H. Frandsen, and P. I. Borel, "Efficient photonic crystal directional couplers," Opt. Lett. **28**(17), 1525–1527 (2003).
32. V. Donzella, S. Talebi Fard, and L. Chrostowski, "Study of waveguide crosstalk in silicon photonics integrated circuits," Proc. SPIE 8915, Photonics North **2013**, 89150Z (2013).
33. S. Xiao, M. H. Khan, H. Shen, and M. Qi, "Modeling and measurement of losses in silicon-on-insulator resonators and bends," Opt. Express **15**(17), 10553–10561 (2007).
34. L. Chrostowski, X. Wang, J. Flueckiger, Y. Wu, Y. Wang, and S. Talebi Fard, "Impact of fabrication non-uniformity on chip-scale silicon photonic integrated circuits," Optical Fiber Communication Conference, pp. Th2A–37, (2014).

1. Introduction

In the last decade, silicon photonics has been a very active and productive research field, with several solutions and systems that have been commercialized [1, 2]. On silicon-on-insulator (SOI) chips, silicon photonics' basic building block is the silicon waveguide, used to transport

#214987 - $15.00 USD Received 1 Jul 2014; revised 7 Aug 2014; accepted 14 Aug 2014; published 22 Aug 2014

and handle light on chips with very low loss (traditional SOI waveguides have a typical propagation loss of about 3 dB/cm [3], that can be reduced up to 0.7 dB/cm [4]). Standard strip (or channel) waveguides for the 1550 nm telecommunication window have rectangular cross-section (220 nm high and 500 nm wide), supporting TE and TM polarized fundamental modes [3,5]. Recently, silicon photonics has also been attracting a great deal of attention as an integrated platform for sensors and lab-on-a-chip devices (LOCs) [6,7]. Silicon photonic components designed for these applications have different requirements than those designed for telecommunications. For example, applications in sensing require a low limit of detection and a high sensitivity and these properties depend on the field penetration into cladding material (the analyte), optical losses, light polarization, etc [8]. Several different solutions have been investigated to improve the performance of waveguide-based silicon photonic sensors, e.g. disks [9], slots [10], Braggs [11], and thin waveguides [12].

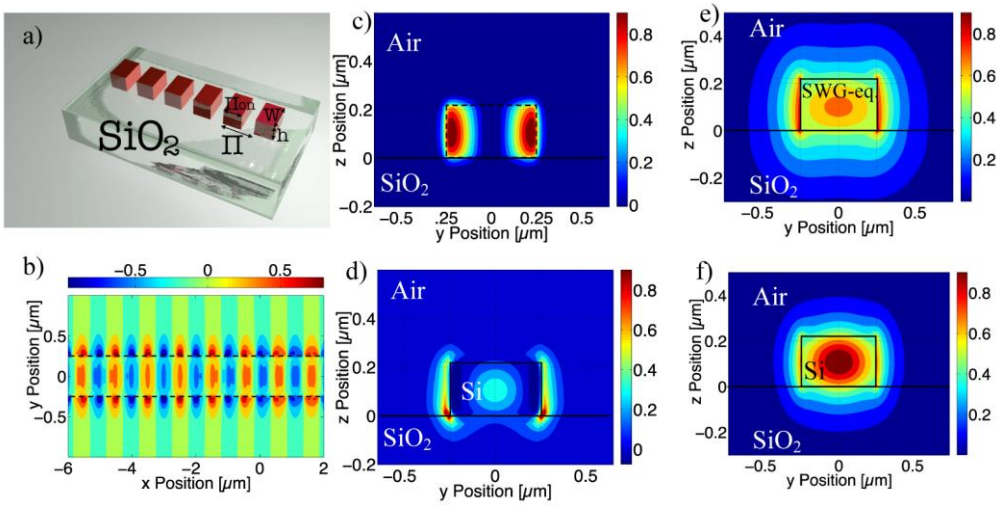

Fig. 1. (a) 3D view of a straight SWG waveguide without top cladding on SOI chip and (b) top view of propagating Re{Ey} field. (b-d) are plots from 3D FDTD simulations of the fundamental TE mode field propagation in the SWG waveguide, (e-f) are plots of the fundamental TE mode profile on the transverse waveguide cross-section using MODE combined with the equivalent refractive index method [21]. SWG electromagnetic field intensity evolution (along one SWG period) on transverse cross-section: (c) field profile in one 'empty space' between two silicon blocks, (d) field profile in a Si block. (e) SWG mode profile, using the equivalent refractive index method and (f) mode in a strip Si waveguide with the same SWG transverse dimensions. SWG shows increased evanescent field penetration into the media (c-e) with respect to traditional waveguides (f). Waveguide cross-section is h = 220nm x w = 500nm, SWG Π = 250 nm.

A very interesting way to customize optical properties is to use sub-wavelength grating (SWG) [13], and SWG-based waveguides were originally proposed as a method for tailoring the core refractive index of a waveguide [14,15], but only very recently have been demonstrated on silicon photonics platform [16]. SWG waveguides are based on periodic structures, but unlike Bragg grating waveguides [17], the gratings are not in a resonant configuration with respect to the wavelength of the propagating light. As a consequence, light propagates like it would in an index-guided structure such as a traditional strip waveguides. The effective refractive index however can be adjusted by choosing the period and duty cycle of the sub-wavelength grating and therefore can be optimized for a given application. One basic way to achieve these structures is to interleave small silicon blocks (with cross-section comparable to traditional waveguides, but each with a length of only a few hundred nanometers) with a lower refractive index material (e.g. SiO_2 or SU-8 like in [16, 18, 19], or air, demonstrated for the first time here) so that the waveguide core is a composite material of

#214987 - $15.00 USD Received 1 Jul 2014; revised 7 Aug 2014; accepted 14 Aug 2014; published 22 Aug 2014

alternating refractive indices [see Fig. 1(a)]. By varying the volume fraction of the two materials in one SWG period (duty cycle), the optical properties of the waveguide can be tuned and optimized for a given application. Light appears to propagate within these waveguides by hopping between the small silicon blocks, as shown by FDTD simulations in Fig. 1(b). These can be simulated as finite-length structures, or as infinite Block-wave structures by considering Block boundary conditions [20].

As already stated, some SWG components have been recently proposed, such as low loss straight waveguides, tapers, multiplexers [16, 18, 19]. In this paper, we demonstrate SWG devices based on the use of air as the lower refractive index core material, with no top cladding. These components are developed for use in sensing applications, particularly when the medium under test is used as a waveguide top cladding. By carefully choosing SWG parameters, light propagation can be guaranteed even if no upper cladding is deposited, as shown in the numerical and experimental results presented in this manuscript. Additionally, we report the theoretical and experimental characterization of a system of basic SWG components, all compatible, that can be used to fabricate all needed and complex integrated optics devices.

The next section will discuss the optical properties of waveguides based on sub-wavelength gratings parameters, then the third paragraph will describe our design methodologies and the fabrication and testing of the devices. Forth, fifth and sixth sections will report main results of simulations and of experimental tests performed on SWG tapers, directional couplers and bends, respectively. Results will be summarized in the last paragraph.

2. Optical properties

SWG propagating mode properties are dictated by the waveguide geometry, the period, Π, of silicon blocks, and the duty cycle, δ, defined as the ratio between the length of silicon core blocks, Π_{on}, and Π. A simplified model for SWG waveguides has been demonstrated and validated previously in [21]. In this model, a SWG can be represented by an equivalent continuous strip waveguide. This equivalent waveguide has a refractive index step of the 'composite core' with respect to the cladding, Δn_{eq}, that can be expressed as a function of the original refractive index step, Δn (the refractive index step between core and cladding of regular strip waveguide), as seen in Eq. (1). This model does not take into account the scattering loss due to the continuous interaction of the field with the walls of the small silicon blocks in the waveguide core.

$$\Delta n_{eq} = \delta \cdot \Delta n \tag{1}$$

The main difference between mode propagation in a traditional strip waveguide and in SWG waveguides is that in the traditional strip waveguide the modal field distribution does not change along the direction of propagation (the mode profile is constant along a strip waveguide cross-section), while the shape and field distribution of the SWG mode changes periodically while propagating (as depicted in Fig. 1(b-d) ; the TE mode profile is shown).

In Figs. 1(e) and (f), we compared TE mode profiles within SOI SWG and strip waveguides with the same transverse cross section of h.220nm x w.500nm, using the equivalent refractive index method. We have chosen not to use any top cladding, demonstrating that SWG confinement can be achieved by exploiting the refractive index contrast between silicon and air (n_{Si} = 3.47, n_{air} = 1). As shown in these mode profiles and in Fig. 2, the SWG waveguide has an enhanced evanescent field [22] with respect to a standard silicon strip waveguide with same cross-section. The evanescent field penetrates deeper in the upper cladding when the SWG duty cycle is smaller, thus a reduced duty cycle means that light confinement in the core is decreased. In turn, having an enhanced evanescent field is very important in sensing applications, in particular when the top waveguide cladding is used as the medium to be analyzed. In addition, there is a significant fraction of the field between the silicon blocks, which can also be used for index sensing (depending on δ, this fraction is

#214987 - $15.00 USD Received 1 Jul 2014; revised 7 Aug 2014; accepted 14 Aug 2014; published 22 Aug 2014

equal to (1-δ)%). The mode profiles in Fig. 1 are extracted from transverse field monitors used in FDTD simulations of a straight SWG waveguide segment. The mode penetration distance is defined as the distance from waveguide surface to have a field reduction of 1/*e*. Values of penetration distance are calculated combining MODE analysis of waveguide transverse cross section with equivalent refractive index method. It is worth noticing that enhancing the evanescent field means also increasing the interaction between the field and the vertical edges of the silicon blocks, and this increased interaction may cause unwanted scattering loss due to wall roughness. Thus, a proper balance between evanescent field and extra loss has to be found depending on the application, in addition, using mature fabrication processes, or reducing writing pitch in the case of E-Beam Lithography can reduce the scattering loss. More details on device fabrication will be given in the next paragraph.

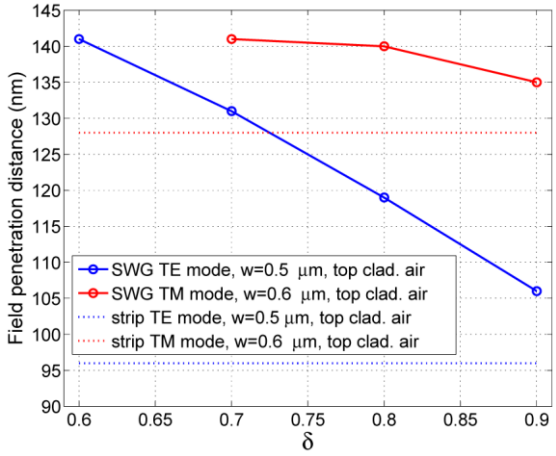

Fig. 2. MODE simulations to evaluate mode penetration distance of the field for SWG waveguides versus SWG duty cycle (continuous lines). Dotted lines are used as comparison with penetration distance of standard SOI waveguides with same transverse cross-section. SWG period is 250 nm, light wavelength is 1550 nm.

Although some SWG components have been demonstrated for devices with SiO_2 or SU-8 top waveguide cladding, e.g. waveguides, edge couplers for coupling light onto the chip from optical fibers, and a broadband directional coupler for strip waveguides [16, 18, 19], several key structures are still missing. Among them, SWG waveguide bends have not yet been demonstrated, nor directional couplers, based on geometries compatible with SWG waveguide mode propagation. In this paper, we report the demonstration of low loss SWG devices, such as straight waveguides, tapers, directional couplers and bends, exploiting air as the low refractive index core material. Presented devices are all based on the same technology and waveguide design, so they are all compatible with the others (Fig. 3), meaning that they can be cascaded and assembled without extra losses. This compatibility is highly desired by silicon photonic designers that can use single components to assemble all photonics devices, with optical properties tailored to the specific application.

#214987 - $15.00 USD Received 1 Jul 2014; revised 7 Aug 2014; accepted 14 Aug 2014; published 22 Aug 2014

3. Design and fabrication

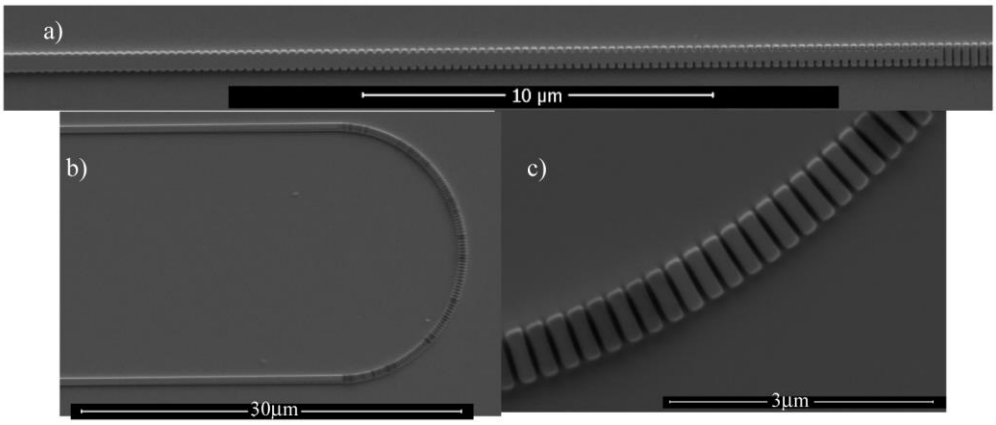

Fig. 3. Fabricated SWG SEM pictures (SWG period is 250 nm, waveguide width is 500 nm): (a) taper detail and (b-c) bend details at low and high magnification, respectively.

We have designed our test structures for bends, directional couplers and tapers using Lumerical FDTD Solutions, as well as the equivalent refractive index method [21] using Lumerical MODE Solutions and FDTD Solutions [23]. Field profile monitors have been used to check and plot propagating and cross-sectional modes in the SWG and its equivalent structures (Fig. 1). Several parameters of fabricated SWG geometries as well as their equivalent refractive index n_{eq} (calculated by adding to the refractive index of the upper cladding Δn_{eq}, accordingly to Eq. (1)) and effective index, n_{eff}, are summarized in Table 1 (the silicon layer height in all cases is the 220 nm foundry standard). n_{eff} has been calculated using the eigenmode solver, defining an equivalent strip waveguide having the same cross section of the SWG building blocks but using a 'user-defined' constant index material with optical properties calculated using the equivalent refractive index method (i.e. the material refractive index is n_{eq}). We have chosen a smaller period combined with a higher δ (0.7-0.8) than what has been used recently for Si SWGs on SOI chips [16, 18, 19], since those two choices have been previously reported as a way to reduce radiation loss [21]. Furthermore, the use of smaller duty cycles would increase the radiation loss of bend waveguides considerably, in particular for smaller radii ($R \leq 20$ µm). It is worth mentioning that the period is upper limited by the Bragg condition $\Pi < \Lambda_B$ [24], because light propagation (with low loss and tailored optical properties) is desired and not light reflection (which introduces extra loss). Λ_B is reported in Table 1 as a comparison with other structure parameters.

Table 1. SWG geometries and optical properties

w (nm)	Pol.	Clad.	Π (nm)	δ (%)	Δn_{eq}	n_{eff}	Λ_B (nm)
500	TE	SiO_2	250	70	1.421	1.71	453
500	TE	SiO_2	250	80	1.624	1.92	405
500	TE	Air	250	70	1.729	1.59	486
500	TE	Air	250	80	1.976	1.82	425
600	TM	SiO_2	250	70	1.421	1.44	538
600	TM	SiO_2	250	80	1.624	1.48	525
600	TM	Air	250	70	1.729	1.43	541
600	TM	Air	250	80	1.976	1.46	531

Devices were fabricated on standard 220 nm silicon on Insulator (SOI) wafers (from Soitech, Peabody, MA), in the University of Washington's Nanofabrication Facility (WNF) using a JEOL JBX-6300FS Direct Write E-Beam Lithography System (EBL) (Peabody, MA). EBL is a faster and reliable fabrication process [25,26], that offers an alternative to long turn around times of many silicon photonics foundries. The standard writing pitch was used for

#214987 - $15.00 USD Received 1 Jul 2014; revised 7 Aug 2014; accepted 14 Aug 2014; published 22 Aug 2014

fabricating our SWG devices, but it is possible to use finer pitches to further improve device writing. All the SWG devices and test structures, including the grating couplers, were fabricated using a single etch writing process. Using a single etch EBL process shortens up the fabrication time, meaning that a standard SOI chip (~2.5x2.5 mm) can be written in few hours (2-4 hours). In the future, compatibility with standard CMOS processes is important for large-scale production, in particular if shorter times of fabrication are required. The small features required for the devices we fabricated (50-100 nm) are challenging for current standard foundry processes, but changing the waveguide geometry, it is possible to have an higher upper limit for the SWG Π, releasing this stringent condition (e.g. one solution might be reducing the waveguide width, keeping constant all the other parameters). Figure 3 depicts SEM images taken from fabricated components, namely of a taper and of a segment of a bend.

The chips were tested using an automated optical test setup, which has been previously described in [8]. This setup allows for the automated interrogation and data acquisition from a large number of devices integrated on a chip in a few hours. Briefly, all the optical (laser, detectors, microscope, etc.), mechanical (micro-positioners, fiber array holder, etc.) and fluidic components (syringe pump) are orchestrated by a dedicated MATLAB software user interface, which is also used for data acquisition. A four-channel polarization maintaining optical fiber array (ports can be used as inputs or outputs, depending on the specific configuration of devices on chip, from PLC Connections, Columbus, OH) is used to couple light from the tunable laser to the chip and to collect the devices' outputs, connecting them to the optical detectors. On chip grating couplers are used to couple light in/out from/to the fiber array [27].

4. SWG waveguides and tapers

The aim of previously developed SWG tapers was to fabricate optimized low-loss edge-couplers from off-chip light sources to on-chip SWG waveguides [19]. The SWGs were used to enhance the mode overlap with the fiber. Here we developed low-loss tapers, for TE and TM polarized light, to transition from devices using strip waveguides to SWG-based devices on the same chip. The modes of the strip and the SWG waveguides are very different, so cascading them without a dedicated taper would cause unwanted extra loss. This effect is shown in Fig. 4(a) that shows the loss due to mode mismatch at the strip to SWG interface (with constant waveguide width). The mode mismatch loss is calculated with MODE. The mode-mismatch loss is more relevant for SWG with smaller δ, and it is polarization dependent (the TM mode is more affected than TE). To avoid an abrupt transition, we designed a taper to gradually modify the SWG core refractive index, to achieve a smooth transition from a SWG mode to a strip mode (or *vice versa*) and to adjust adiabatically the mode size. To generate a smoother transition from SWG to strip waveguide, bridging silicon elements are added in the taper structure, between SWG silicon blocks, so the equivalent refractive index is progressively increased to match strip n_{eff} [inset of the schematic taper structure is in Fig. 4(b)].

Figure 4(b) presents the total taper loss (with bridging elements), from SWG to strip (and *vice-versa*) waveguide for TE and TM modes. The taper loss has been evaluated by 3D FDTD, and the taper shape is the same as used for the masks for fabrication (Fig. 4(b) inset). 3D FDTD simulations clearly show that the smooth core index variation reduces mode-mismatch loss, in particular for SWGs with lower δ, which have a higher difference between the effective indices of the modes at the two ends of the tapers. The simulated total taper loss for the TM mode (red curve) is smaller than that for the TE (blue curve), and this is likely due to the fact that the difference between n_{eff} of the TE mode in strip and in SWG waveguides is about five times higher than the same difference for TM mode. As such, the TM mode transition is remarkably smoother than the TE one, since we kept the taper length fixed to 30 μm for both polarizations. This taper length was a good compromise between taper loss (from

#214987 - $15.00 USD Received 1 Jul 2014; revised 7 Aug 2014; accepted 14 Aug 2014; published 22 Aug 2014

simulations the total loss is always lower than 0.5 dB) and taper footprint. Obviously, depending on design and space requirement, it is possible to further minimize the taper loss. The TM mode has a reduced interaction with sidewalls, thus is less affected by scattering loss due to the discontinuities of the SWG core. These smoother transitions of TM modes as compared to TE are consistent with our experimental observations. On the other hand, we simulated a TE taper with doubled taper length (blue dotted plot, total taper length in this case is 60 μm) in order to generate a smoother transition for the TE mode. In this case, the taper loss is slightly decreased with respect to the shorter taper, thanks to the improved transition, but for larger duty cycles (when the mode mismatch is reduced) propagation loss begins to dominate over mode mismatch loss. Indeed, for duty cycle 0.9 the propagation loss is one order of magnitude bigger than for δ = 0.8, for TE mode, as shown in Fig. 4(c).

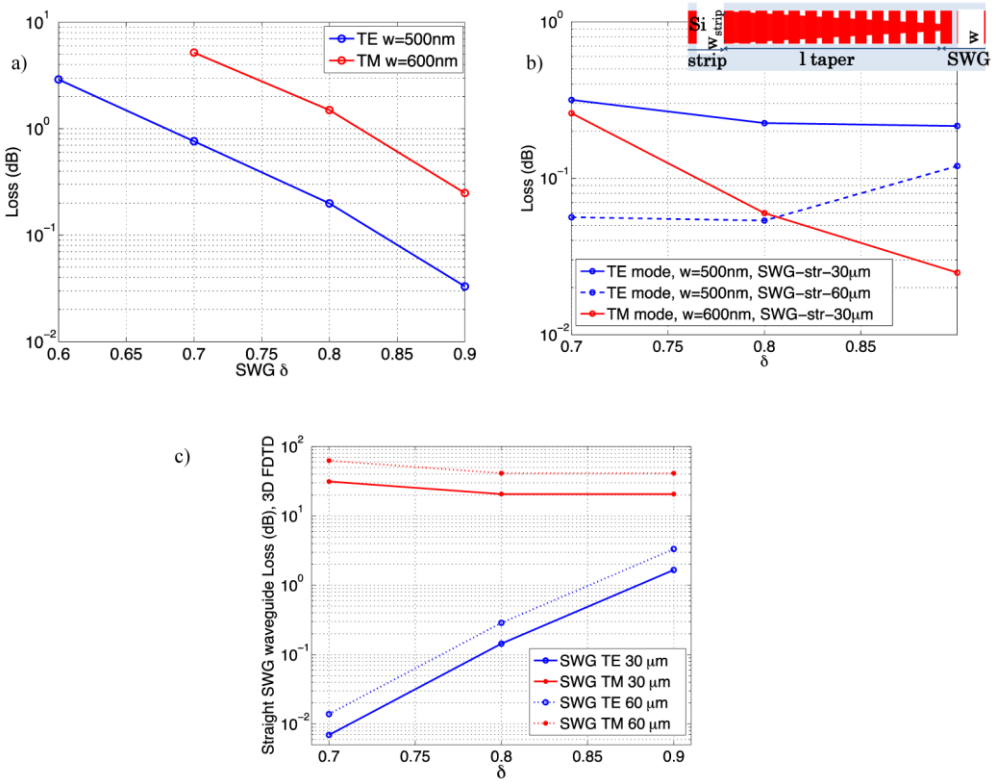

Fig. 4. (a) Simulated mode mismatch loss (MODE simulation) between input and output taper modes (TE and TM) vs. SWG δ, The SWG period is 250 nm. Top cladding is air, λ = 1550nm. (b) 3D FDTD simulation of total taper loss vs. SWG δ for SWG to strip waveguide transition and different modes (TE mode is in blue while TM is in red). For TE mode it is shown the effect of having a longer taper (dotted blue line). Inset shows taper top view, not at scale. (c) 3D FDTD simulation of straight SWG waveguide loss, for a 30 μm long (continuous line) and for 60 μm long waveguide (dotted lines). TE mode related curves are blue while TM curves are red. In the 3 graphs, waveguide cross-section is h = 220nm x w = 500nm (TE) or w = 600nm (TM).

We have fabricated SWG taper test structures, varying the number of tapers in the link and keeping all other structure parameters constant; the single taper loss was extracted from the measurements of several of these structures. We fabricated test structures for TE and TM modes with two duty cycles (0.7 and 0.8), but unfortunately all experimental results for TM SWGs with δ = 0.7 show very high total taper loss (likely due to scattering loss due to core discontinuities that are higher than in simulations, Fig. 4). Because of the extent of these

#214987 - $15.00 USD Received 1 Jul 2014; revised 7 Aug 2014; accepted 14 Aug 2014; published 22 Aug 2014

losses we could not use them in our characterization. In Fig. 5 we reported experimental results for fabricated tapers and their comparison with simulations. Figure 5(a) presents the spectra of cascaded TM tapers for increasing number of tapers (from 2 up to 24), and $\delta = 0.8$. We subtracted from received spectra the spectrum of the grating coupler link [27], to analyze any frequency dependence in the taper response. The link with only two tapers cascaded does not present a significant wavelength dependence; this is interesting considering the fact that in a simple mixed link with SWG and strip waveguides, no frequency dependence is introduced by converting these waveguides. On the other hand, if the link is more complex, the introduction of multiple gratings, and multiple reflection paths between them, can cause unwanted loss and wavelength dependence in the optical link response. The inset in the figure shows the total loss for each test structure, calculated from the experimental results, along with a linear data fit that can be used to extract experimental loss per taper as shown in Fig. 5(b). Figure 5(b) reports measured and simulated taper loss for TE and TM mode vs. duty cycle. Simulations are in agreement with measured data, but there is an underestimation of the total experimental loss per taper of about 0.4 dB, and this is likely due to the fact that 3D FDTD simulations do not take into account for scattering loss, that in SWG structures is emphasized by sidewall roughness and fabrication imperfections. As predicted by simulations, the total TM taper loss is smaller than the TE one, thanks to a lower difference between effective indexes at the input and output of the taper.

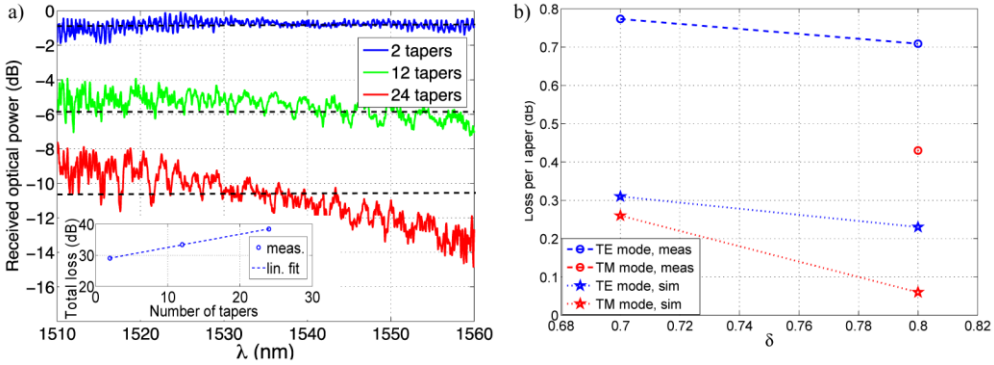

Fig. 5. (a) Normalized received spectra of TM cascaded SWG/strip waveguide tapers for increasing taper number, inset reporting the measured total loss as a function of number of tapers, with linear fit to extract the single taper loss. The spectra are normalized with respect to the optical link on chip without any taper. Dotted black lines represent the loss values extracted from the fit for 2,12 and 24 cascaded tapers. (b) Taper loss from experimental and simulated results, TE and TM mode, vs. SWG duty cycle.

5. SWG directional coupler

Directional couplers are widely used in integrated optics, to act as optical switches [28], to couple light into resonators [29], to direct different wavelengths in demultiplexers [30], etc. The basic directional couplers have a simple design (two parallel segments of waveguides separated by a gap) but have a disadvantage of having a wavelength dependent coupling coefficient. More complex designs are often used to mimic the simple function of directional couplers with improved performance [31], but they usually loose the ease of fabrication and compactness. A simple combination of SWG and traditional strip waveguides has been recently proposed [18] to have a directional coupler for strip waveguides with fivefold gain in bandwidth without increasing device size. Here, we present the study and fabrication of a SWG directional coupler, aimed to be compatible with all SWG components presented in this manuscript. The structure of the designed directional coupler is shown in the SEM picture in Fig. 7(a).

#214987 - $15.00 USD Received 1 Jul 2014; revised 7 Aug 2014; accepted 14 Aug 2014; published 22 Aug 2014

The SWG directional coupler for TE mode shows a significant decrease in wavelength dependence as seen in Fig. 6(a). The cross over length, L_c is defined as the length the light would have to travel to be entirely coupled into the second waveguide. It is calculated using MODE simulations of the effective indices of the symmetric and anti-symmetric coupler modes [32]. The crossover length, L_c, dependence on wavelength for different duty cycles, δ, is reported in Fig. 6(b), (other SWG parameters are kept constant, and the coupling gap, g, is 200 nm). These results indicate that smaller duty-cycles offer improved performance, in terms of a dramatically reduced cross-over length dependence on signal wavelength. This can also be explained by looking at the simulated effective refractive index. For smaller duty cycles the effective index decreases and hence the light is less confined and therefore has a stronger coupling to a waveguide in proximity.

$$\kappa_{meas} = \sqrt{\frac{P_{coupled}}{P_{in}}} \tag{2}$$

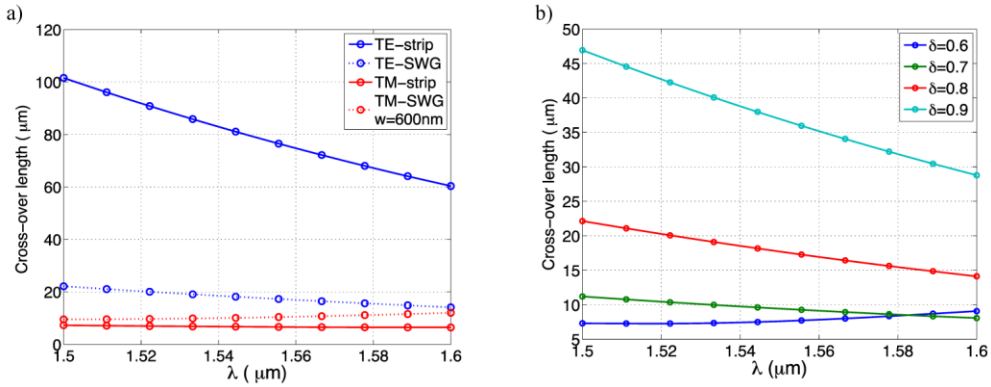

Fig. 6. (a) Comparison of cross-over length, L_c, dependence on wavelength of input light for SOI strip (continuous lines) and SWG waveguides (dotted lines). SWG duty cycle is 0.8. (b) L_c for SWG directional coupler with different δ, TE mode, g = 200nm, waveguide parameters are kept constant. If not specified, waveguide cross-section is h. 220nm x w. 500nm, Π = 250nm and coupling gap, g = 200nm. Top cladding is air.

$$L_{c-meas} = \frac{\pi \cdot L_{coupler}}{2 \cdot \arcsin(\kappa_{meas})} \tag{3}$$

Simulation results are confirmed by experimental data; the coupler behavior is almost constant versus wavelength (on a span of more than 40 nm). In Fig. 7(b) we report the experimental $L_{c\text{-}meas}$ (extracted from TE mode measurements of a directional coupler with a gap of 200 nm) versus wavelength, for two duty cycles (δ = 0.7,0.8). The coupling coefficients were calculated from the measured power in the two outputs of the directional coupler [Eq. (2)]; these coupling coefficients were used to evaluate the effective coupling length (Eq. (3), where κ_{meas} is the field coupling coefficient from Eq. (2), and $L_{coupler}$ is the length of the straight segment of the directional coupler). The experimental results are very close to the simulated ones [dotted lines in Fig. 7(b)], and the extracted cross-over length is almost constant in the measurement region. On the other hand, the simulated L_c showed a decreasing linear dependence on wavelength, as in regular strip waveguides, thus this discrepancy can be due to neglected radiation loss in the simulations in the equivalent refractive index model. The design is targeted to work at λ = 1550nm; at this wavelength the simulations and the measurements are in good agreement, in particular for the SWG waveguide with larger δ (= 0.8). In this case, a higher SWG duty cycle leads to a stronger field confinement in the SWG core (see also Fig. 2) reducing radiation loss, as described in

#214987 - $15.00 USD Received 1 Jul 2014; revised 7 Aug 2014; accepted 14 Aug 2014; published 22 Aug 2014

[20]. As the crossover length L_c is almost constant in the analyzed wavelength range, so is field coupling coefficient, κ, of the fabricated directional coupler.

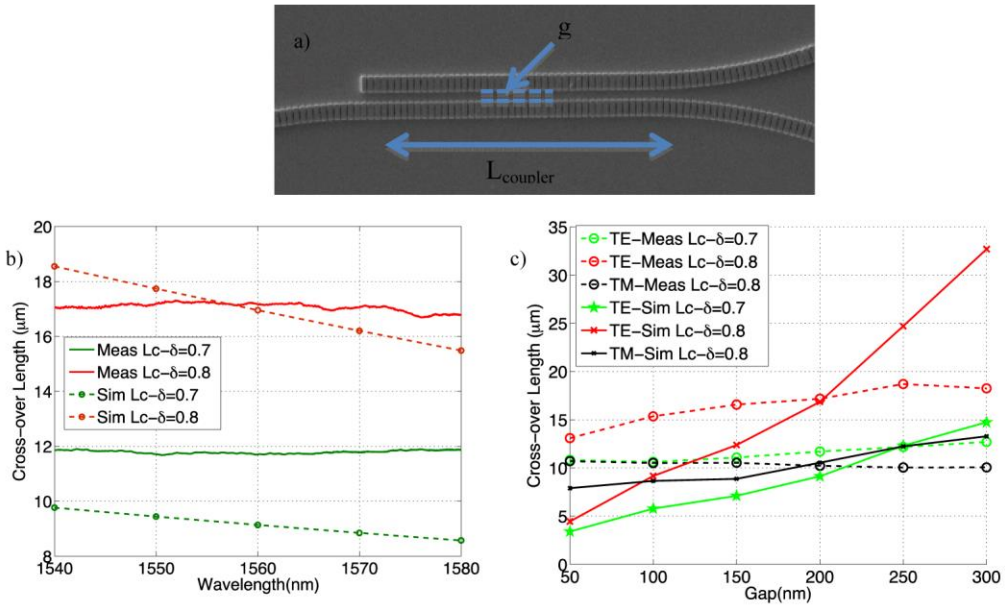

Fig. 7. (a) SEM picture of a directional coupler, with some parameters highlighted. (b) Comparison of L_c dependence on input light wavelength for TE SOI SWG directional couplers. Continuous lines indicate $L_{c\text{-}meas}$ values calculated from measurements using Eqs. (2)-(3) and dotted ones stand for simulated results. The power of the two output ports is normalized with respect to the total output power. In (a) and (b) SWG is h.220nm x w.500nm, Π = 250nm, g = 200nm. Top cladding is air, and duty cycles indicated in figure. (c) Experimental evaluation of coupler $L_{c\text{-}meas}$ vs. gap compared with L_c simulation results. In (b) and (c) simulated results were generated using MODE, equivalent refractive index method and theoretical evaluation [32]. For TM light, w = 600nm.

Finally, Fig. 7(c) reports L_c values calculated from measurements of SWG directional couplers with different gaps, different duty cycles and for TE and TM polarizations (dotted lines in figure). These results are compared with simulations. Lumerical MODE is used, combined with the equivalent refractive index method. Simulations are in good agreement with measurements for TM mode and TE mode in SWG with smaller duty cycle, while there is a noticeable difference between measurements for the SWG directional coupler with bigger duty cycle (δ = 0.8). It is worth noticing that the equivalent refractive index method is a simplified model of SWG waveguides, as explained in [21], thus it is valid to have a preliminary estimation of waveguide parameters. In order to include in the simulations the effect of radiation loss, a 3D FDTD model can be used (obviously, it is remarkably more time consuming). Nonetheless, scattering loss is included neither in FDTD nor in MODE simulations, and it can play a key role when etches features are very small (e.g. for δ = 0.8). A more accurate scattering loss modeling may be required in extreme cases, but it is outside the aim of this paper.

6. SWG bends

To the authors' knowledge, SWG bends have not yet been demonstrated; previous work on SWG has focused on straight segments of SWG components [16, 18, 19]. When bends are needed as basic building blocks for more complex optical structures, they are fabricated using standard strip waveguides. The use of standard strip bends requires extra tapers (between SWG and strip waveguides and *vice versa*), thus wasting space on chip and introducing extra

#214987 - $15.00 USD Received 1 Jul 2014; revised 7 Aug 2014; accepted 14 Aug 2014; published 22 Aug 2014

loss in the optical link (each strip bend requires two tapers in an SWG-based optical link). Waveguide bends are an essential optical component for silicon photonics chips, especially if SWG-only devices are required. Bends are also required to build up more complex devices, such as resonators, interferometers, modulators, etc. In this paper we report the fabrication of SWG bends, and analyze their performance with 3D FDTD simulations. It is worth noting that in our layout we have regularly used SWG bends, e.g. for connecting directional coupler input and outputs to the relative GCs [Fig. 7(a)], so we are also demonstrating the possibility of cascading in a functional way the different components we are characterizing in this paper. Investigated SWG bends have the same period used for the other components already presented in this paper (Π = 250 nm) and the same cross-section dimensions (500 nm x 220 nm for the TE mode). Again, we varied the duty cycle (δ = 0.7, 0.8) and used no top oxide cladding.

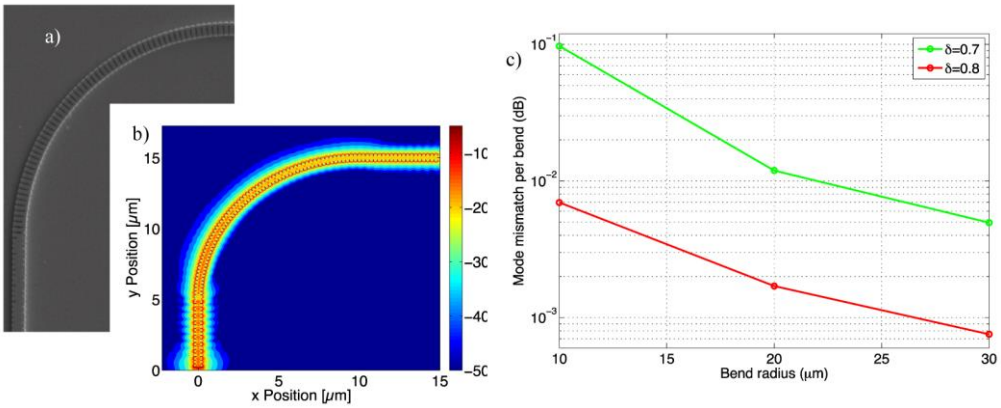

Fig. 8. (a) SEM picture of 10 μm SWG bend on SOI chip, with δ = 0.8 and Π = 250nm, and (b) top view of Re{E} propagating in this kind of bend calculated via 3D FDTD for λ = 1550 nm, TE mode. (c) Mode mismatch loss calculated by equivalent refractive index method and MODE, versus bend radius for two different SWG duty cycles. In all the simulations waveguide cross section is h. 220 nm x w. 500 nm and SWG Π = 250 nm.

Figure 8(a) shows the SEM picture of an SWG bend (R = 10 μm, δ = 0.8) on SOI chip and Fig. 8(b) depicts the absolute value of the electric field calculated via a 3D FDTD simulation of the same bend. In the simulations, light is injected from the SWG straight waveguide segment at the bottom left of the simulation region; the source central wavelength is 1550 nm. The source is placed in the middle of a silicon block of the SWG waveguide core, but it is injecting the fundamental mode of regular silicon strip waveguide, thus at the beginning of the SWG waveguide there are some losses due to mode mismatch and reflections, visible in the bottom left corner of Fig. 8(b). SWG waveguide parameters are the same as those used for the other devices already presented in this paper. Simulations show that, with an appropriate SWG duty cycle, light propagates with the typical mode periodicity of SWG waveguides. In Fig. 8(c) we evaluated the mode mismatch loss using the equivalent method and MODE solutions, as already described earlier. The mode mismatch loss decreases when the radius increases; indeed in smaller bends the mode is more delocalized with respect to the SWG straight waveguide mode [3]. The mode mismatch decreases for bigger δ, since the equivalent refractive index is higher, thus the mode is more confined. Based on simulation results, and in particular noticing that bends with small δ (e.g. δ<0.7, combined with R = 10 μm) do not propagate light (that is radiated out from the bend structure), we fabricated bend loss test structures with cascaded SWG bends. In particular we have cascaded four SWG bends in a resonating configuration, and extracted the bend loss from the quality factor of the resonators, using the method described in [33].

#214987 - $15.00 USD Received 1 Jul 2014; revised 7 Aug 2014; accepted 14 Aug 2014; published 22 Aug 2014

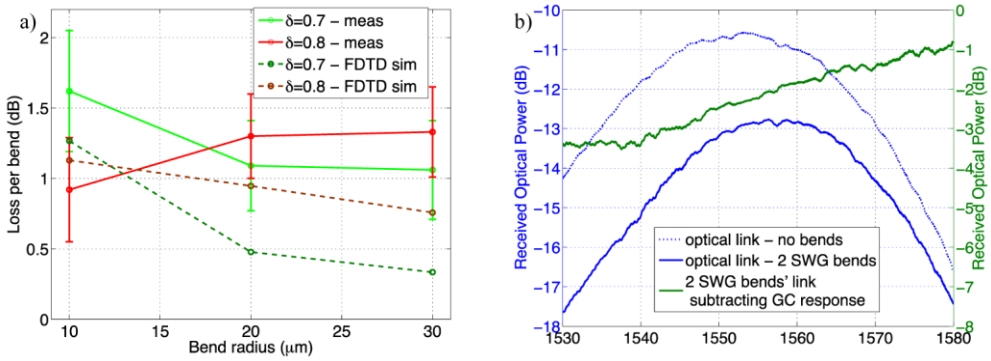

Fig. 9. (a) Bend loss versus radius of experimental results (continuous lines, with mean value and error bars) compared with simulations (dotted lines), different duty cycles are shown with different colors. (b) Spectra of two similar optical links, one without any bend and one with two SWG bends cascaded (left axis), and spectra of the two SWG bends normalized with respect to the GC optical link (right axis); R = 10 μm and δ = 0.8. In all cases waveguide cross section is h. 220 nm x w. 500 nm and SWG Π = 250 nm.

The total bend loss for SWG waveguides was evaluated using input and output monitors in the 3D FDTD simulations of a 90° bend, taking the ratio between the power measured by the two monitors. The results of bend loss evaluated for TE bends are presented in Fig. 9(a), dotted lines. The radius is increased from 10 μm to 30 μm with 10 μm steps, and two duty cycles are reported, with different colors. From simulations, the loss per bend decreases when the radius increases, like the mode mismatch loss shown in Fig. 8(c), thus for smaller radii we expect that radiation and mode mismatch loss are the dominant causes of loss. On the other hand, the total loss per bend is higher for bigger δ, suggesting that increasing the duty cycle may cause extra bend loss that can be attributed to scattering and radiation. The continuous lines in Fig. 9 (a) depict the mean loss value, with error bars, calculated from repeated measurements on the bend test structures for the two different duty cycles, overlapped with the simulation results. Mean bend loss extracted from experiments are slightly higher (in the range of 0.3-0.7 dB of difference) than simulated one, in all cases but one (δ = 0.8 and R = 10 μm), but the values are in good agreement taking into account measurement errors and the fact that there is a certain variability of devices' parameters along the chip [34]. The slight underestimation of loss in simulations is reasonable, since the fabricated SWG devices must have extra loss due to sidewall roughness, accentuated by fabrication imperfections. The trends of the loss, decreasing with increasing radii, and lower loss for smaller duty cycles, are consistent between simulations and experiments.

Figure 9(b) reports the spectrum of two cascaded SWG bends compared with the spectrum of the same optical link without the bends. The SWG bends have R = 10 μm and δ = 0.8. It is clearly shown that the bends introduce a remarkable loss in link, but we have two take into account that in the second link we have also two SWG-strip tapers, which increases the total loss of the link (of about 0.5-0.6 dB). The measured power decrease is comparable with the experimental results we have achieved for tapers [Fig. 5(b)] and bends [Fig. 9 (a)].

7. Conclusions

We have presented, analyzed and discussed several SWG components, realized on silicon on insulator chips. Devices were fabricated with no upper cladding and measured in air for the first time for SWG based components on SOI chips. The bends, tapers and directional couplers, are compatible one with one another and with SWG straight waveguides, and can be used to build up more complex SWG based devices and optical links. The use of SWG based components allows for having devices with optical properties different from standard SOI waveguides, thus enhanced flexibility of the design and also possibility to explore novel

#214987 - $15.00 USD Received 1 Jul 2014; revised 7 Aug 2014; accepted 14 Aug 2014; published 22 Aug 2014

application such as biosensors. Devices were simulated and optimized using the equivalent refractive index method combined with modal analysis (performed with Lumerical MODE) as well as 3D FDTD. Then devices were fabricated on standard SOI chips via electron beam lithography and tested with our automated optical test setup. Measurements are in good agreement with simulation results for all the devices presented in the paper, and results are promising in terms of use of optical links completely based on SWG and tailored to specific needs and applications. Fabricated SWG directional couplers have a wavelength flattened response on a bandwidth of more than 40 nm, bends have a loss around 1 dB per bend, and tapers (to convert SWG to strip waveguides) have a loss that is lower than 0.8 dB per taper in all the cases analyzed. Although the values of losses reported for the described devices are relatively low, allowing the cascade of several SWG devices in optical links, they are higher with respect to components based on traditional SOI strip waveguides. Nonetheless, the loss of fabricated SWG devices are still higher than simulated values, showing the possibility of further improvement. One interesting approach can be to fabricate them with processes ensuring very low wall roughness (e.g. using smaller writing pitches for EBL), to reduce scattering due to the augmented interaction of the electromagnetic field with silicon block walls in the core. Furthermore, the loss is obviously related to the enhanced evanescent field, so, depending on the application, an optimal balance loss-field penetration distance can be found by changing the SWG parameters. Another approach to reduce loss, which has been already demonstrated, can be to use an upper cladding as such as silicon dioxide, but this solution hinders the possibility to use SWG devices for label-free sensing. In conclusion, our devices demonstrate their potential for use in optical link with applications that are not restricted to telecommunications wavelengths, but thanks to their flexible design they can be of remarkable importance for microsystems and sensing and different project requirements.

Acknowledgments

The authors would like to thank CMC Microsystems, Mentor Graphics, Lumerical Solutions, Inc. for providing the simulation software. We are grateful to John Bock for his inspiring presentation on sub-wavelength gratings. We gratefully acknowledge the Centre for High-Throughput Phenogenomics at the University of British Columbia (UBC) for assistance with SEM imaging. We are also grateful to Prof. NAF Jaeger at UBC for his insights and support. We gratefully acknowledge NSERC CREATE Silicon Electronic Photonic Integrated Circuits (SiEPIC) training program. This work was made possible by a National Priorities Research Program grant from the Qatar National Research Fund. Devices were fabricated by Richard Bojko, at the University of Washington Nanofabrication Facility (WNF), a member of the NSF National Nanotechnology Infrastructure Network.

#214987 - $15.00 USD Received 1 Jul 2014; revised 7 Aug 2014; accepted 14 Aug 2014; published 22 Aug 2014